Research Square

Preprints are preliminary reports that have not undergone peer review.
They should not be considered conclusive, used to inform clinical practice,
or referenced by the media as validated information.

Surface Assembling of Individual Probiotics with pH-Responsive Epigallocatechin Gallate Nanoparticles against DSS-induced colitis

Suqing Lan
Zhejiang University
Jike Shuai
Zhejiang University
Ziyang Deng
Zhejiang University
Yunxuan Li
Zhejiang University
Yi Wang
Zhejiang University
Donghong Liu
Zhejiang University
Xingqian Ye
Zhejiang University
Shiguo Chen
chenshiguo210@163.com
Zhejiang University
Haibo Pan
Zhejiang University

Article

Keywords: EGCG nanoparticles, Assembling of probiotics, Escherichia coli Nissle 1917, Lactobacillus plantarum, Colitis

Posted Date: March 26th, 2026

DOI: https://doi.org/10.21203/rs.3.rs-9109800/v1

License: This work is licensed under a Creative Commons Attribution 4.0 International License.
Read Full License

Additional Declarations: No competing interests reported.

Abstract

Probiotics are potential treatments for inflammatory bowel diseases, but their efficacy is primarily restricted by the adverse gastrointestinal conditions that limit activity and adhesion. In light of the high bioactivity and the strong absorption onto mucus layer and bacterial surface of polyphenols, it's of considerable interest in developing a polyphenol-based collaborative platform to coat probiotics for improved efficacy. Here, we developed a single-cell coating strategy with polyphenol nanoparticles self-assembling on cellular surface through Mannich reaction-induced self-assembly of polyphenols. Polyphenols adhering on bacterial cells underwent a Mannich condensation reaction to produce oligomeric derivatives, which assembled to generate nanoparticles through intermolecular entanglement and interaction via primarily hydrophobic π − π stacking and intermolecular hydrogen bonds. Probiotics were coated individually with the self-assembled nanoparticles in 30 min. The pH-responsive nanoparticles kept stable at low pH (2–6) and disassembled at high pH (7–9), resulting in improved probiotic viability against acidic gastric fluid and bile salts, and enhanced colonization in the intestinal tract without loss of proliferation capabilities. Furthermore, the polyphenols can also trigger significant antioxidant, anti-inflammatory, and barrier-protective effects, thereby synergizing with probiotics to alleviate colitis in mice. This surface self-assembling strategy represents a robust platform to enhance the potency of probiotics for the treatment of ulcerative colitis.

Introduction

Intestinal microorganisms are closely associated with various physiological and pathological processes, including host cell proliferation, neural signal transduction, bone density and hormone biosynthesis.[1–3] When the gut environment is disturbed by endogenous or exogenous factors, such as pathogens, antibiotic treatment, or diet, intestinal dysbiosis may occur, triggering inflammation or even cancer. In contrast, the oral intake of adequate probiotics can help restore microbial balance and confer health benefits to the host. As a result, the global market for probiotic foods and beverages continues to expand and is projected to grow from $42.5 billion in 2017 to $94.4 billion in 2024.[4] However, oral probiotic delivery encounters multiple challenges: the low pH of gastric acid, the antimicrobial effects of bile salts, and degradation by lipases markedly reduce probiotic viability.[5,6] Moreover, effective adhesion to the intestinal epithelium is essential for sustained colonization.

Recently, a variety of cell encapsulation technologies, such as microcapsules, hydrogels, liposomes, emulsions and membranes, have been developed.[7–11] Microencapsulation remains the most widely used method, typically employing extrusion, emulsification, and spray drying techniques with polysaccharides and proteins as matrix materials for sol-gel fixation, ionic condensation, or emulsion polymerization.[12] Although these approaches offer partial protection, issues persist, including limited size control, leakage, low in-vivo colonization efficiency, and incompatibility with food matrices.[13,14] Bulk encapsulation embeds probiotics within nanoscale gel matrices, whereas single-cell encapsulation forms nanometer-thick coatings on individual cells. Compared with multicellular encapsulation, single-

cell encapsulation significantly enhances biological activity and enables more effective cellular-level interventions.[15]

Microorganisms in nature have evolved continuously to adapt to a series of harsh environments. For instance, *Bacillus su btilis* forms endospores with stress resistance to counteract adverse conditions, including drying, heating, radiation, and oxidation. Based on such biological characteristics, a series of biomimetic methods have been adopted to construct artificial shells for the purpose of single-cell encapsulation, aiming to reduce the damage caused by the external environment to cells and add additional biological functions.[16–18] Materials like silica, graphene, dopamine, and metal-polyphenol networks have already been applied to single-cell encapsulation, and these materials share the common feature of not affecting cell activity. The layer-by-layer assembly technology (LBL) usually relies on the electrostatic attraction generated when probiotics are alternately exposed to coating materials with negative and positive charges.[19] Self-assembly refers to the behavior of molecules spontaneously arranging into an orderly hierarchical structure.[20] Cell-surface functionalization and coordination-driven assembly are also common single-cell encapsulation techniques. Compounds containing catechol or gallic acid functional groups are well-known for their antioxidant, adhesive, and metal chelating capabilities.[21] In recent years, the multifunctional coordination chemistry of metal-phenol network (MPN) represented by tannic acid, epigallocatechin gallate (EGCG), and Fe^{3+} has become a crucial synthetic strategy for surface engineering. However, MPN has pH responsiveness and will disassemble under acidic conditions, which reduces its protective effect under the condition of gastric acid and consequently fails to promote the colonization of probiotics in the intestine.

In this study, we proposed a method for assembling probiotics with polyphenol-amino acid nanoparticles. Two model probiotics, *Escherichia coli* Nissle 1917 (EcN) and *Lactobacillus plantarum* GDMCC 1.140 (Lp), were engineered using a simple but effective nano-assembly strategy. As illustrated in Scheme 1, EGCG was first adsorbed onto the bacterial surface. In the presence of aldehyde groups, glycine was then added to initiate a Mannich condensation reaction, forming linear oligomeric derivatives of tea polyphenols. As the reaction progressed, intermolecular hydrogen bonding and π–π stacking interactions strengthened, promoting the entanglement of these oligomers. Ultimately, the oligomers self-assembled on the bacterial surface, forming nanoparticles (NPs).[22] These NPs exhibit distinct pH responsiveness: they remain stable and protective under acidic gastric conditions but disassemble under alkaline intestinal conditions. Following NPs disassembly, polyphenols remain adhered to the probiotic surface, preserving bacterial proliferation while facilitating adhesion to the intestinal epithelium and exerting synergistic anti-inflammatory effects. Polyphenols containing pyrogallol groups (such as EGCG and tannic acid) strongly interact with intestinal mucins through the Michael addition reaction, thereby enhancing probiotic colonization and reinforcing the mucus barrier. Additionally, by modulating gut microbial composition, polyphenols promote the production of short-chain fatty acids (e.g., butyrate), which exhibit antioxidant, anti-inflammatory, and barrier-protective functions, ultimately alleviating intestinal inflammation and tissue damage.[23] EGCG is also a natural plant-derived prebiotic with excellent biosafety. Therefore, this study systematically evaluates the

protective effects of this assembly strategy in vitro and in vivo, along with its capacity to promote intestinal colonization and mitigate dextran sulfate sodium (DSS)-induced colitis.

Results and Discussion

Preparation and Characterization of Assembled Probiotics

Among these polyphenol-mediated interactions, the phenolic hydroxyl groups have good adhesion properties to plenty phenolic hydroxyl groups providing tissue adhesive.[24] Owing to the general surface binding affinity of EGCG, this method proves applicable to a diverse range of bacteria.[25] As depicted in Fig. 1a, in contrast to naked bacteria, the UV-VIS spectra of EcN and Lp with EGCG adhered to their surfaces exhibit absorption peaks near 235 nm and 273 nm, which result from electron transitions caused by the intramolecular conjugated structure.[26] The adhesion of EGCG represents the initial step of the assembly process. Subsequently, glycine is introduced, and in the presence of aldehyde groups, the Mannich reaction takes place. Initially, linear tea polyphenol oligomeric derivatives are generated. Subsequently, due to the augmentation of intermolecular hydrogen bonds and π-π stacking forces, the intermolecular entanglement and interaction of the derivatives intensify, ultimately leading to the self-assembly of these oligomers on the bacterial surface to form EGCG-glycine nanoparticles.[22] This process can be completed within approximately 30 min. Subsequently, the surplus reactants are removed via centrifugation to obtain the assembled bacteria. The FT-IR spectra of the nanoparticles and the two types of assembled bacteria, along with the naked bacteria, are presented in Fig. 1b. After the condensation reaction forms nanoparticles, characteristic absorption peaks emerge at 1204 cm^{-1} (C-N-C) and 1118 cm^{-1} (C-O-C), whereas the naked bacteria lack obvious absorption peaks at these two locations.[27] This preliminarily indicates that the assembly reaction transpires on the bacterial surface to form nanoparticles.

To validate that the assembly of these nanoparticles occurs on the bacterial surface, rhodamine-B is utilized to stain EGCG-nanoparticles. Through non-covalent interactions, functionalized polyphenol nanoparticles are obtained, thereby giving rise to a fluorescence phenomenon.[28] Observation using CLSM reveals that, due to the presence of nanoparticles on the surfaces of the assembled bacteria, conspicuous fluorescence signals can be discerned, while no fluorescence is observable on the naked bacteria. SEM images demonstrate that, in comparison with the naked bacteria, spherical nanoparticles are attached to the surfaces of the assembled bacteria. Moreover, the length of the bacteria is augmented by around 0.5-1 μm, and their morphology appears more intact. While confirming the success of the assembly, it also implies that the nanoparticles possess a protective effect during the vacuum pumping process. Additionally, TEM analysis indicates that due to the existence of NPs on the surfaces of the assembled bacteria, the surfaces of the bacteria become thicker. This leads to a larger electron scattering angle, fewer electrons passing through, darker image brightness, and a hemispherical shape around them.[29]

Finally, the particle size and potential of the nanoparticles (NPs), naked bacteria (EcN and Lp), and assembled bacteria (EcN-NPs and Lp-NPs) are measured by dynamic light scattering. In Figure S1, the average particle size of the NPs is 487.1 ± 13.1 nm, that of EcN is 830.1 ± 40.2 nm, that of EcN-NPs is 988.3 ± 26.9 nm, that of naked Lp is 714.7 ± 35.3 nm, and that of Lp-NPs is 873.0 ± 21.1 nm. When compared with the naked bacteria, the average particle sizes of the assembled bacteria all display a significant increase. The Zeta potential of NPs was similar to that of EcN, and there was no significant difference between them, which indicates that the nanoparticles did not alter the surface potential characteristics of EcN during the assembly process. However, the situation with Lp was different. Due to the significant difference in Zeta potential between NPs and Lp.[30] After evaluating the growth and vitality of the assembled bacteria, it is concluded that this assembly method does not exert a significant inhibitory effect on the growth of the bacteria (Figure S2).

Owing to the linear relationship between the concentration of nanoparticles and the optical density at OD_{660}, it can be effectively utilized for the preliminary determination of the disassembly rate of NPs under varying pH conditions.[31] As illustrated in Fig. 2a-c, when the pH is set at 2 and 3 respectively, the average disassembly rates of the nanoparticles amount to 11.0% and 6.8%. Nanoparticles maintain their structural integrity and exhibit no disassembly within the pH range of 4 to 5. At pH 6, the disassembly rate reaches 8%. In solutions with a pH spanning from 7 to 9, the nanoparticles undergo complete disassembly, assuming a brownish and transparent configuration. Probiotic products are customarily administered postprandially, and at this stage, the acidity of the gastric juice contents approximates 3.[32] Under such acidic circumstances, the nanoparticles can retain their essential form and execute a protective function. They will disassemble in the intestinal fluid with a pH of 7, liberating probiotics and eliciting a synergistic anti-inflammatory effect between probiotics and polyphenols. Concurrently, polyphenols can also enhance the colonization efficacy of probiotics in the intestine.

Within the human physiological context, antioxidants assume a crucial role in attenuating the risk of diseases by alleviating oxidative stress.[33] Previous investigations have established that EcN and LP are probiotics that are highly esteemed for their remarkable antibacterial, anti-inflammatory, and microbiota homeostasis-regulating attributes and are extensively employed in the treatment of a spectrum of gastrointestinal maladies.[34] In light of the fact that polyphenols possess robust free radical scavenging and antioxidant potencies, we further delved into whether the assembled bacteria could possess augmented antioxidant capacities and consequently mitigate the symptoms of DSS-induced colitis in mice.[35] The antioxidant activities of the assembled bacteria and their naked counterparts were evaluated via ABTS and DPPH free radical scavenging assays, and the results were graphically presented in a visually intuitive manner. According to the data presented in Fig. 2d-e, with Trolox (TE, a water-soluble analogue of vitamin E) serving as a reference standard, both EcN-NPs (0.84 mmol Te) and Lp-NPs (0.75 mmol Te) demonstrated superior free radical scavenging capabilities in comparison to EcN (0.27 mmol Te) and Lp (0.19 mmol Te). As a result, the ABTS scavenging rates of Ec and Lp subsequent to assembly were enhanced by 46.1% and 45.8% respectively. As depicted in Fig. 2f-h, DPPH was employed as a probe to explore the proficiency of the assembled bacteria in scavenging DPPH free

radicals. In the reaction system, the purple coloration in the solutions of the assembled bacteria groups faded prominently, and the absorbance value at 519 nm diminished significantly, thereby indicating that the assembly of probiotics with polyphenol nanoparticles led to a substantial augmentation in the ability to eliminate DPPH free radicals. Before and after assembly, the DPPH scavenging rate of EcN was elevated from 1.7% to 42.1%, and that of Lp was increased from 2.6% to 50.0%. These findings suggest that the assembly of probiotics with polyphenol nanoparticles not only bolsters their free radical scavenging capabilities but also augments the survival prospects of probiotics in oxidative stress responses.

In Vitro Resistance of Assembled Probiotics against Gastrointestinal (GI) Tract

It is a well-recognized fact that the low pH level of gastric juice poses the primary and most formidable obstacle for orally administered probiotics, given its propensity to inactivate cells on a considerable magnitude.[36] Thereupon, two probiotic strains were conjugated with nanoparticles. Following the treatment in simulated gastric juice (pH = 2) fortified with pepsin, a plate counting assay was carried out, and their growth trajectories were scrupulously surveilled. In consonance with the data illustrated in Fig. 3a, after being exposed to the treatment in simulated gastric fluid (SGF) for a duration of one hour, the viability of the EcN plummeted from 9.0 Log_{10} CFUs to 5.2 Log_{10} CFUs. Conversely, the viability of the EcN-NPs attained 6.4 Log_{10} CFUs. Analogously, as in the case of the two-hour treatment in SGF, the assembly maneuver efficaciously augmented the survival rate of probiotics under acidic circumstances. Subsequently, the growth kinetics of the bacteria subsequent to SGF treatment was scrutinized. It was discerned that, in juxtaposition to the uncoated bacteria, the nanoparticle-assembled bacteria manifested a more expeditious growth rate and could reach the stationary phase with greater celerity (Fig. 3b). In contradistinction to EcN, the one-hour and two-hour treatments in SGF had a negligible influence on the survival rate of Lp. Nevertheless, it did impinge on the tempo at which it reached the stationary phase. Precisely, the longer the treatment time, the more sluggish the growth of the bacteria. The survival rate of Lp before and after assembly was approximately enhanced by a factor of 20 (Fig. 3c-d).

Bile salts, which possess the capacity to solubilize lipids, and pancreatic enzymes endowed with enzymatic hydrolysis capabilities were incorporated into the simulated intestinal fluid (pH = 7) to explore the activities of the uncoated bacteria and the nanoparticle-assembled bacteria. As delineated in Fig. 3e-f, the nanoparticle-assembled bacteria evinced a remarkably enhanced resistance to simulated intestinal fluid (SIF) in comparison with the uncoated bacteria, with the effect being particularly conspicuous for Lp. During the spot plate enumeration on the plate, under the identical dilution concentration, the assembled bacteria exhibited a more copious number of colonies and a higher bacterial density. The coated bacteria and the uncoated bacteria were successively treated with simulated gastric juice for two hours and then with simulated intestinal fluid for two hours, trailed by live/dead cell staining (Figure S3-S4). As a corollary, more than half of the uncoated bacteria expired during the treatment process. In contrast, the preponderant majority of the nanoparticle-assembled bacteria retained their viability and aggregated in a clustered fashion, which might potentially be ascribed to the intrinsic viscosity of the

nanoparticles. The previous studies was predicated on the acid disassembly property of most probable number and was ameliorated through layer-by-layer assembly (LBL), which customarily demanded several days for material preparation and assembly consummation.[37–39] In the present study, the self-assembly of probiotics with nanoparticles could be effected within one hour in a single step, thereby fortifying their survival rate.

The Survival and Colonization Status of Assembled Probiotics in Vivo

Since it has been previously demonstrated that assembly can enhance the activity of probiotics in SGF under *in vitro* conditions. Moreover, the EGCG molecule contains multiple phenolic hydroxyl groups, which are capable of forming hydrogen bonds with certain components on the surface of the intestinal mucosa, such as proteins and carbohydrates. For instance, the mucus layer on the intestinal mucosa mainly consists of glycoproteins. The phenolic hydroxyl groups of EGCG can interact with the hydroxyl or amino groups in glycoproteins through hydrogen bonds, thereby augmenting its adhesiveness in the intestine.[40] Additionally, the molecular structure of EGCG is relatively large and possesses a specific spatial conformation. This structural characteristic enables it to better combine with the irregular structures on the intestinal surface, just like a specially designed "key" that can match the "lock" on the surface of the intestinal mucosa. In the alkaline intestinal environment, the deprotonated phenolic hydroxyl groups are more favorable for binding with positively charged intestinal mucosal proteins, thus enhancing its adhesiveness.[41]

Based on the aforementioned experiments and facts, we employed the chemical transformation method to introduce the plasmid pBBR1MCS2-TacmCherry (with kanamycin resistance) into EcN, and consequently obtained naked bacteria and assembled bacteria that are capable of expressing red fluorescent protein (as illustrated in Figure S5). Mice were orally gavaged with 1×10^9 CFUs. Subsequently, the mice were sacrificed at 4, 24, 48, and 96 h, and the gastrointestinal tissues were extracted. The distribution of probiotics *in vivo* was observed using the *in vivo* fluorescence imaging system (IVIS), and the number of viable bacteria in the contents of the stomach, intestine, cecum, and colon was enumerated respectively. As depicted in Fig. 4a, 4h after oral gavage, in the stomach, small intestine, and colon, the number of viable bacteria in the assembled bacteria group was 10–15 times that of the naked bacteria group, and it was approximately 40 times higher in the cecum. Notably, no viable bacteria were counted in the small intestine of the naked bacteria group starting from 24 h, while there were still 3.6 Log_{10} CFUs in the assembled bacteria group (Fig. 4b). At 48 h (Fig. 4c), the assembled bacteria also effectively exerted the protective effect. In Fig. 4d, 96h after oral administration, no viable bacteria were detected in the gastrointestinal tract of the assembled bacteria group, but there were still 2.4 Log_{10} CFUs and 2.3 Log_{10} CFUs of probiotics in the cecum and colon of the assembled bacteria group.

The retention of naked bacteria and assembled bacteria in the gastrointestinal tract of mice at 4 h, 24 h, and 48 h was visualized by IVIS, as shown in Fig. 4e. Unlike the aforementioned plate counting results of the gastrointestinal contents, fluorescence expression was still observable in the small intestine of the

naked bacteria group after 24 h, suggesting that a small quantity of bacteria remained. The possible reason for this discrepancy is that IVIS imaging was carried out immediately after the mice were sacrificed, without subjecting the probiotics to mechanical damage. In contrast, during the sampling and homogenization of the contents for plate counting, some bacteria were inactivated. In the mice orally gavaged with assembled bacteria, from 4 h to 48 h, it could be seen that the blue area in the stomach became progressively lighter, while the cecum and colon regions began to turn blue, indicating that the probiotics in the stomach were gradually transported to the colon and cecum through the small intestine for colonization and proliferation. In the experimental control group, where the mice were gavaged with naked bacteria, as time elapsed, the content of probiotics in the stomachs of the mice gradually decreased, but there was no significant increase in the colon and cecum. This might be due to the inactivation of most of the naked bacteria by gastric acid or their failure to colonize successfully in the mice and subsequent excretion out of the body along with metabolites.

All these results clearly indicate that assembly remarkably improves the oral bioavailability of EcN in the gastrointestinal tract, including the survival rate and colonization rate of probiotics.

Preventive Efficacy of Assembled Probiotics against DSS-Induced Colitis in Mice

In the aforementioned experimental investigations, the satisfactory survival and colonization rates of the assembled bacteria, both in the *in vivo* and *in vitro* settings, have impelled us to conduct a more in-depth exploration regarding the prophylactic efficacy of Armed EcN against DSS-induced colitis. A cohort of fifty mice, after a 7-day acclimatization period, was randomly segregated into five distinct groups, namely the CK, DSS, NPs, EcN, and EcN-NPs. Subsequently, over a consecutive 14-day period, the mice were administered daily intragastrically with 200 μl aliquots of water, nanoparticle solution, naked bacteria, or assembled bacteria, respectively. On the 7th day of the experiment, with the exception of the CK, the drinking water was supplanted with a 1.5% DSS solution to instigate colitis induction (Fig. 5a)[42]. At the culmination of the experimental protocol, the mice were euthanized, and their colons, spleens, cecal contents, and sera were harvested for further comprehensive analysis.

As depicted in Fig. 5b, upon termination of the experiment, in comparison to the control group, the body weight of the mice in the model group exhibited a reduction of 11%, whereas that of the assembled bacteria group only declined by 4%. This finding unequivocally suggests that the assembled bacteria possess the capacity to mitigate the body weight loss in mice consequent to DSS exposure. However, no statistically significant differences in body weight alterations were discernible between the nanoparticle group, the naked bacteria group, and the model group. The Disease Activity Index (DAI) is a composite scoring metric that takes into account body weight loss, fecal consistency, and the presence of hematochezia.[43] Based on the DAI scores of the four experimental groups, it was evident that, in contrast to the nanoparticle and naked bacteria groups, the assembled bacteria manifested a more pronounced alleviative effect on fecal consistency and hematochezia (Fig. 5c). During the initial 7-day phase, the body weights of the mice demonstrated a gradual increment. Two days following DSS

intervention, the body weights of the DSS-treated groups initiated a downward trajectory. As the modeling duration extended, the body weights of the mice in the model group underwent a significant reduction. Seven days post-intervention, a statistically significant disparity in body weight was observed between the model group and the control group. Moreover, based on the DAI values, a preliminary determination of successful modeling could be made.

Intestinal inflammation is invariably associated with colon shortening and an elevation in the spleen enlargement index.[44] The mean length of the colon in the control group was measured at 7.86 ± 0.68 cm, in contrast to 5.24 ± 0.74 cm in the model group. The nanoparticle and naked bacteria groups exhibited colon lengths of 5.46 ± 0.63 cm and 6.13 ± 0.69 cm, respectively, whereas the assembled bacteria group registered a mean length of 6.91 ± 0.54 cm. In comparison to the naked bacteria group, the assembled bacteria group exhibited a more substantial ameliorative effect on colon shortening in mice (Fig. 5d-e).Analyzing the final spleen index (Fig. 5f), it was revealed that, relative to the control group, the spleen index of the model group was significantly augmented. The nanoparticle and assembled bacteria groups were efficacious in alleviating the spleen enlargement in mice induced by DSS, whereas the naked bacteria group failed to demonstrate any discernible effect.

The H&E staining results presented in Fig. 5i illustrated that the epithelial cells and crypt structures of the colon tissues in the healthy mice of the control group were intact, devoid of any inflammatory cell infiltration. Conversely, the colons of the mice in the model group manifested irregular morphological characteristics, with a majority of the crypt structures obliterated, goblet cell damage, and pronounced inflammatory cell infiltration. Employing the pathological scoring criteria for colon tissues to quantitatively assess the ulcerative conditions of the colon tissues in each group, the results, as depicted in Fig. 5g, indicated that nanoparticles, naked bacteria, and assembled bacteria were all capable of ameliorating the ulcerative symptoms of the colon tissues in mice, with the assembled bacteria group exhibiting the most prominent effect. Mucus, secreted by goblet cells, constitutes the primary physical defense mechanism within the intestinal barrier. It functions to segregate microorganisms within the intestinal lumen from host epithelial cells, thereby precluding direct contact of bacteria, toxins, and antigens with the epithelial cells.[45] AB staining enables the visualization of acidic mucoproteins as dark blue, thereby permitting the determination of the distribution and expression levels of mucoproteins in colon tissues. Through the utilization of image processing software to calculate the proportion of the mucoprotein area in each group, it was established that the NPs, EcN, and EcN-NPs groups were all effective in mitigating the destruction of the mucus layer and the reduction of goblet cells associated with DSS-induced colitis (Fig. 5h and 5j).

Lipopolysaccharide (LPS), a prevalent endotoxin, gains access to the systemic circulation subsequent to damage of the intestinal barrier.[46] This event triggers the generation of copious amounts of inflammatory mediators and instigates a cascade of reactions within the organism. LPS and lipopolysaccharide-binding protein (LBP) are recognized as crucial indicators of intestinal leakage.[47] In Fig. 6a-b, the LPS and LBP levels in the mouse sera were quantified using enzyme-linked immunosorbent assay (ELISA) to appraise the integrity of the mouse colon barrier. The results demonstrated that the

EcN-NPs > EcN > NPs. Tumor necrosis factor-alpha (TNF-α) (which induces ROS production and epithelial necroptosis), interleukin-6 (IL-6) (which promotes intestinal inflammation by activating antigen-presenting cells and T cells), and interleukin-1β (IL-1β) (which induces the expression of multiple inflammation-related genes) are acknowledged as pro-inflammatory cytokines in the pathogenesis of ulcerative colitis and can provide a partial reflection of the degree of intestinal inflammation.[48–50] In contradistinction to pro-inflammatory factors, IL-10 serves as a pivotal regulator of the intestinal mucosal immune response. It functions to inhibit antigen presentation and the release of pro-inflammatory cytokines, thereby attenuating mucosal inflammation and is regarded as a paradigmatic anti-inflammatory factor in the colitis model.[51] As illustrated in Fig. 6c-f, NPs, EcN, and EcN-NPs were all capable of significantly diminishing the levels of pro-inflammatory factors and promoting the release of anti-inflammatory factors, with the assembled bacteria group exhibiting the most remarkable effect. The up-regulation of anti-inflammatory factors and the suppression of pro-inflammatory factors both contribute to the amelioration of DSS-mediated colon injury and the inhibition of the further progression of inflammation.

It is a well-established fact that the gut microbiota of patients afflicted with inflammatory bowel disease (IBD) frequently exists in a state of imbalance. Oral probiotics represent a commonly employed approach for rectifying the gut microbiota of IBD patients. Consequently, this study harnessed 16S rRNA sequencing to investigate whether oral administration of nanoparticles, naked probiotics, and assembled probiotics could confer protection against DSS-induced colitis in mice.

The rarefaction curves presented in Fig. 6g indicated that, as the volume of sequencing data progressively increased, the number of newly identified operational taxonomic units (OTUs) gradually declined and approached a plateau, thereby attesting to the rationality of the sequencing data obtained in this experiment and the capacity of the sequencing results to mirror the preponderant biological information within the samples. Chao1 is intimately correlated with community richness, while the Shannon index and Simpson index are reflective of the species diversity within the community. The results demonstrated that the Chao1 index of the gut microbiota of the mice in the control group was conspicuously higher than that of the model group, and statistically significant differences were observable between the model group and the experimental groups. This implies that nanoparticles, naked bacteria, and assembled bacteria exert a significant impact on the preservation of the richness of the gut microbiota in colitis mice (Fig. 6h). The Shannon index results of the gut microbiota of the mice in each group were congruent with the Chao1 index, but no significant differences in the Simpson index were detected among the groups (Fig. 6i and S7).

PCoA, a dimensionality reduction technique predicated on the Weighted Unifrac distance algorithm, was employed to dissect the associations among the microbiota of the mice in each group (Fig. 6j). A greater inter-point distance corresponded to a diminished correlation between the samples. It was manifest that the model group deviated substantially from the control group, corroborating the disruption of the gut microbiota in mice with DSS-induced colitis. In contrast, the assembled bacteria group exhibited a near congruence with the healthy mice in the control group, substantiating the capacity of intragastric

administration of assembled bacteria to reverse the structural imbalance of the gut microbiota in colitis mice.

A further analysis of the mouse gut microbiota at the phylum level was performed, and the results are presented in Figure S8. As depicted in Fig. 6k, within the assembled bacterial consortium, the preponderant genera include *Prevotellaceae*. This genus is commonly regarded as being related to a wholesome plant-based diet and functions as "probiotics" in the human body, facilitating the breakdown of protein and carbohydrate-based foods. Another significant genus is *Lachnosporaceae* of the *Allobaculum* genus, which has the ability to decompose certain carbohydrates that are otherwise indigestible by the human body, generating short-chain fatty acids like butyric acid.[52] This process is beneficial in preventing obesity and colon cancer. *Muribaculaceae* is also among the beneficial bacteria, being renowned for its anti-inflammatory properties.[53] Furthermore, the administration of the assembled bacteria via gavage can lead to a reduction in the presence of *Escherichia-Shigella*, a typical intestinal pathogen known to accumulate in inflamed mucosae. It can also decrease the levels of *Enterorhabdus*, for which prior research has indicated a certain degree of correlation with spontaneous colitis in mice. In addition to these, other harmful bacteria associated with IBD are also diminished in colitis mice.[54]

To specifically compare the taxonomic differences in the microbiota among groups, Fig. 7 presents the LEfSe (Linear Discriminant Analysis Effect Size) analysis results of the mouse gut microbiota.

By setting the LDA score threshold, 21 bacterial taxa that were significantly enriched in different groups were identified. Specifically, the characteristic genera of the model group, naked bacteria group, assembled bacteria group, and nanoparticle group were *Desulfovibrionaceae*, *Bacteroidaceae*, *Lachnospiraceae*, and *Oscillospiraceae*, respectively.Among these, *Desulfovibrionaceae* are sulfate-reducing bacteria (SRB). They utilize sulfate as an electron acceptor for respiration instead of oxygen. In the intestinal environment, *Desulfovibrionaceae* produce hydrogen sulfide (H_2S) through sulfate reduction. Studies have shown that the accumulation of H_2S is considered toxic to intestinal epithelial cells, and thus associated with the development and persistence of IBD. In contrast, *Bacteroidaceae*, *Lachnospiraceae*, and *Oscillospiraceae* are generally recognized to exert beneficial effects on intestinal health. In conclusion, intragastric administration of nanoparticles, naked bacteria, and assembled bacteria all played a positive role in regulating the gut microbiota and maintaining intestinal health in mice. Among them, the assembled bacteria exhibited superior efficacy in ameliorating the gut microbiota dysbiosis in DSS-induced colitis mice, demonstrating greater therapeutic potential.

Conclusion

Prior investigations have established that, the assembly process can enhance the activity of probiotics in SGF, and EGCG can augment the adhesion of probiotics within the intestine. Through the chemical transformation method, naked bacteria and assembled bacteria capable of expressing red fluorescent protein were obtained and administered to mice via gavage. *In vivo* experiments demonstrated that at each time interval following oral gavage, the viable count, survival rate, and colonization rate of the

assembled bacteria in the gastrointestinal tract were markedly higher than those of the naked bacteria. IVIS imaging further revealed that the assembled bacteria exhibited favorable colonization in mice, in contrast to the relatively poor performance of the naked bacteria. This indicates that the assembly process significantly improves the oral bioavailability of EcN in the gastrointestinal tract. In the DSS-induced colitis experiment, the assembled probiotic group was effective in alleviating the weight loss of mice and demonstrated a prominent effect in relieving symptoms such as fecal stickiness and bloody stools. Compared with other groups, it was more proficient in mitigating colon shortening and splenomegaly. Indicators such as the pathological score of colon tissues and the proportion of mucin area also attested to the assembled bacteria having the most favorable improvement effect on colitis. In terms of inflammatory factor detection, the assembled probiotic group exhibited the most pronounced effect in reducing the levels of pro-inflammatory factors and promoting the release of anti-inflammatory factors. The results of 16S rRNA gene sequencing indicated that nanoparticles, naked bacteria, and assembled bacteria had a significant impact on maintaining the richness of the intestinal flora of mice with colitis, and the assembled probiotic group could reverse the structural imbalance of the flora in these mice. Its dominant genera, including *Prevotella*, *Allobaculum*, and *Lachnospira*, play crucial roles in intestinal metabolism, immune regulation, and other aspects, further corroborating the beneficial effect of the assembled bacteria in preventing DSS-induced colitis and their positive influence on the intestinal microecology.

Looking ahead, these research achievements regarding assembled probiotics have paved the way for extensive applications of probiotics in the health domain. On the one hand, there is anticipation for further refinement of the formulation and preparation procedures of assembled probiotics, aiming to further enhance their activity, colonization rate, and efficacy within the human gastrointestinal tract. This would enable the development of more efficacious probiotic preparations for the prevention and adjunctive treatment of diverse intestinal disorders, such as inflammatory bowel disease and irritable bowel syndrome, thereby alleviating patient suffering and enhancing their quality of life. On the other hand, delving deeper into the interaction mechanisms between assembled probiotics and the intestinal microbial community holds the potential to offer novel concepts and methodologies for personalized medicine and precision nutrition. Tailored probiotic therapies could be devised based on the unique characteristics of an individual's intestinal flora, enabling precise modulation and maintenance of intestinal health, fostering the elevation of the overall health status of the human body. Additionally, this would provide robust scientific backing for the innovative advancement of functional foods and health products.

Methods

Materials: *Escherichia coli* Nissle 1917 (EcN) and *Lactobacillus plantarum* GDMCC 1.140 were obtained from China Center of Industrial Culture Collection (CICC, China). 98% of epigallocatechin gallate (EGCG) was purchased from Shanghai Darui Fine Chemical Co., Ltd. Formaldehyde (analytical reagent, AR) was purchased from HuShi. Glycine and rhodamine B were bought from Aladdin. The agar and liquid media of LB and MRS were purchased from Solarbio. DPPH, pepsin and trypsin were all bought from Macklin.

The ABTS kit for detecting antioxidant activity was purchased from Beyotime. The pBBR1MCS2-Tac-mCherry plasmid used for transformation was purchased from Wuhan Miaoling Biotechnology Co., Ltd.

Animals: C57BL/6 mice were purchased from Hangzhou Qizhen Laboratory Animal Technology Co., Ltd. DSS (molecular weight 35,000–50,000 Da) was provided by MP Biomedicals, USA. SPF-grade AIN-93G purified feed was supplied by Nanjing Synergy Biotech Co., Ltd. All animal experiments were reviewed and approved by the Institutional Animal Care and Use Committee of Zhejiang Laboratory Animal Center.

Culture and preservation of bacteria: *Escherichia coli* Nissle 1917 (EcN) and Lactobacillus plantarum were stored in LB and MRS broths containing 50% glycerol, respectively, and frozen at -80°C. For all culturing steps, a single colony of EcN was inoculated into LB broth and grown overnight at 37°C. Then, 100 μL of the overnight culture was transferred to fresh LB broth and grown overnight at 37°C with shaking at 220 rpm in a shaking incubator for formal experiments. A similar protocol was applied to the growth of Lactobacillus plantarum using MRS broth.

Assembly of bacteria: 4 mL of the bacterial suspension was centrifuged at 5000 rpm for 5 minutes. After removing the supernatant, the pellet was resuspended in deionized water, and this process was repeated three times. Finally, the pellet was resuspended in 40 mL of deionized water. Subsequently, 122 mg of epigallocatechin gallate (EGCG), 30 μL of formaldehyde, and 30 mg of amino acids were added successively. After mixing thoroughly, the reaction was allowed to proceed at room temperature for 1 hour. Then, the mixture was centrifuged at 5000 rpm for 5 minutes to remove excess reactants, obtaining the assembled bacteria.

Measurement of ultraviolet spectra: The bacterial suspension was centrifuged at 5000 rpm for 5 minutes. After removing the supernatant, the pellet was resuspended in deionized water, and this was repeated three times. EGCG solution (3 mg/mL) was added to the bacterial pellet, mixed for 5 minutes, and then centrifuged at 5000 rpm for 5 minutes. After removing the supernatant, the pellet was resuspended in deionized water, and this was repeated three times. Finally, it was resuspended in an equal volume of deionized water. Two kinds of bacteria with EGCG adhered to the surface were obtained, using the aqueous solutions of bacteria and EGCG solution as controls.

Detection of infrared spectra: The prepared assembled bacteria, naked bacteria, and nanoparticle samples were pre-frozen in a -80°C freezer and then freeze-dried in a vacuum dryer. 1 mg of each group of samples and 99 mg of dried potassium bromide were ground in one direction and then sampled on a mold. The mixture was compressed into a glassy thin slice and measured in the range of 400–4000 cm^{-1}. Data were collected by 32 scans with a 4 cm^{-1} resolution.

Confocal laser scanning microscopy imaging: In the above bacterial assembly process, EGCG was replaced with rhodamine B-labeled EGCG, while the other assembly processes remained unchanged. After preparation, 20 μL of the sample was dropped onto a glass-bottomed culture dish. After standing for one minute, the fluorescence phenomenon was observed under a confocal laser scanning microscope.

Scanning electron microscopy imaging: 10 μL of the diluted sample was dropped onto a silicon wafer on the carrier plate, naturally dried in a clean bench for 30 minutes, and then sputter-coated with gold for observation.

Transmission electron microscopy imaging: The sample was diluted 10 times. A copper grid (with a front and a back side) was picked up with tweezers and immersed in the sample. Excess liquid was absorbed with the edge of filter paper. Then, a drop of 1% uranyl acetate was added, and the excess stain was absorbed. After waiting for 30 minutes, the sample was observed.

Measurement of particle size and zeta potential: For particle size measurement, the sample was diluted 30 times and then added to the particle size cell. The average hydrated particle size of the sample was determined by the dynamic light scattering method in a laser nanoparticle size analyzer. For zeta potential measurement, 0.9 mL of the sample solution was pipetted into the DTS1070 potential cell, and the Zeta potential of the sample was measured in the Zetasizer Nano Lab potential analyzer. All measurements were carried out at 25°C with an equilibration time of 120 seconds. Each measurement was performed 12 times and repeated 3 times.

pH responsiveness of nanoparticles: An ultraviolet-visible spectrophotometer (Persee, TU-1901, China) was used to record the change in optical turbidity (OD value) of the nanoparticle solution at 660 nm. A linear relationship between nanoparticle concentration and optical turbidity was obtained ($y = 0.8823x + 0.1176$, $R^2 = 0.9907$), so as to detect the disassembly rate of nanoparticles at different pH values.

Antioxidant capacity (DPPH method): The OD600 of the assembled and unassembled probiotics was adjusted to approximately 1.0 with PBS. Then, aliquots were added to 0.2 mM DPPH ethanol solution (19.716 mg of DPPH was weighed and dissolved in ethanol solution, and the volume was fixed to 250 mL with absolute ethanol solution. The ratio of sample to DPPH ethanol solution was 1:2 v/v) and mixed thoroughly. The mixture was allowed to stand at 37°C in the dark for 30 minutes. Control reactions were prepared with deionized water and ethanol. The absorbance of each mixture was quantified at 531 nm. The antioxidant activity was calculated using the following formula: scavenging effect (%) = (Ac - As)/Ac × 100, where As is the absorbance of the test sample and Ac is the absorbance of the control at 531 nm.

Antioxidant capacity (ABTS method): Equal volumes of ABTS solution and oxidant solution were mixed and stored in the dark for 12–16 hours to prepare the ABTS stock solution. Then, the stock solution was diluted with PBS (about 32 times) so that the absorbance at 734 nm measured by a microplate reader was 0.75 ± 0.05. 200 μL of ABTS working solution was added to a 96-well plate, mixed well, and then 10 μL of each group of samples was added. After standing at room temperature for 10 minutes, the absorbance at 734 nm was measured. Asample is the nanoparticle solution at different concentrations, Acontrol is the methanol nanoparticle solution at different concentrations, and A0 is the ABTS solution only. The total antioxidant capacity was referenced to the concentration of vitamin E. The scavenging rate formula is as follows:

$$Y = \left\{1 - \frac{A_{\text{sample}} - A_{\text{control}}}{A_0}\right\} \times 100\%$$

In vitro digestion simulation: Equal amounts of naked bacteria and assembled bacteria were immersed in simulated gastric fluid (SGF) (0.2% NaCl, 3.2 g/L pepsin, HCl, pH 1.2) for 1 hour or 2 hours, respectively. Then, the survival amount and growth vitality of the treated bacteria were detected, so as to obtain the protective effect of assembly on bacteria in simulated gastric fluid. The protection in simulated intestinal fluid was achieved by treating the bacteria in simulated intestinal fluid (SIF) (0.68% KH_2PO_4, 10 g/L trypsin, NaOH, pH 6.8) for 2 hours, and then counting the viable bacteria. After continuous treatment in simulated gastric fluid for 2 hours and then in simulated intestinal fluid for 2 hours, the viability of bacteria after *in vitro* digestion simulation was observed under a confocal laser scanning microscope using live-dead dyes.

In vivo colonization and adhesion experiment: The pBBR1MCS2-Tac-mCherry plasmid was transformed into competent *Escherichia coli* Nissle 1917 and cultured in a medium containing 50 μg/mL kanamycin to obtain EcN that could express red fluorescent protein. In animal experiments, male C57BL/6 mice aged 6–8 weeks were gavaged with 1 × 10^8 CFUs of naked EcN-mCherry or assembled bacteria, respectively. At 4, 24, 48, and 96 hours after gavage, the stomach, small intestine, and large intestine of the mice were dissected out, and fluorescence imaging of the entire gastrointestinal tract was performed using the IVIS imaging system. The contents in the above gastrointestinal tissues were homogenized with 2 mL of PBS and then diluted and spread on LB agar plates containing 50 μg/mL kanamycin for CFU counting. Thus, the activity differences of bacteria or assembled bacteria in different gastrointestinal tissues at different times were obtained.

In vivo prevention of colitis experiment: 50 male C57BL/6 mice were randomly divided into 5 groups after 7 days of acclimation, namely the control group, model group, nanoparticle group, naked bacteria group, and assembled bacteria group. Mice in the control group and model group were gavaged with 200 μL of water daily for 2 consecutive weeks. The nanoparticle group was gavaged with 0.2 mg of nanoparticles. The naked bacteria group was given 5 × 10^8 CFU of naked EcN, and the assembled bacteria group was given 5 × 10^8 CFU of assembled bacteria. In the latter four groups, the drinking water was replaced with 1.5% DSS solution in the second week to induce acute colitis in mice. After the start of the experiment, the body weight changes of the mice were recorded daily. On the last day of the experiment, the mice in the experimental groups were scored for the DAI according to body weight loss scores, feces consistency, and bloody stools.

Colon length, spleen index: When dissecting the mice, the spleen, colon, and cecum of the mice were removed. The length of the colon was photographed and measured, and the spleen was weighed. The spleen index was calculated according to the following formula: spleen index (SI) = spleen mass (mg)/body weight (g) × %. Then, the contents of the colon and cecum were taken into cryotubes, respectively. A 1-cm distal colon was fixed in Carnoy's fixative for histopathological examination, and the remaining colon tissue was placed in a cryotube.

Histopathological observation of colon tissue: The colon tissue fixed in 4% paraformaldehyde (or Carnoy's fixative) was paraffin-embedded, sectioned, and stained with hematoxylin and eosin reagents. An inverted microscope was used to observe and collect colon section photos magnified 4 times and 40 times. The colon tissues of each mouse were scored according to the histopathological scoring criteria. The histological damage score of each mouse was the sum of crypt destruction, goblet cell damage, and inflammation.

Serum inflammatory factor analysis: Blood collected by orbital bleeding was allowed to stand for 2 hours and then centrifuged at 3000 rpm for 15 minutes at 4°C to collect serum. Then, the serum was divided into two parts, one was frozen for storage, and the other 100 μL was used for subsequent detection. Referring to the steps in the ELISA kit, the levels of TNF-α, IL-1β, 6, 10, LPS, and LBP in the mouse serum were measured by Jiangsu Enzyme Label Biotechnology Co., Ltd., and the corresponding contents were calculated through the standard curve.

Changes in microbiota richness: Mouse colon content samples were sent to Beijing Novogene Technology Co., Ltd. for microbiota DNA extraction, quality identification, and composition analysis. The hypervariable regions V3 - V4 of the bacterial 16S rRNA gene were amplified using specific primers 338F (5'-ACTCCTACGGGAGGCAGCAG-3') and 806R (5'-GGACTACHVGGGTWTCTAAT-3'). The amplification products were sequenced by high-throughput sequencing on the Illumina NovaSeq platform and analyzed by bioinformatics. Gene sequences were merged using FLASH (v 1.2.8), and sequences with more than 97% similarity were classified into OTU.

Declarations

Supporting Information

The Supporting Information is available free of charge.

Competing interests

The authors declare no competing interests.

Author Contribution

S.L.: Investigation, data curation, formal analysis, writing—original draft, visualization. J.S.: Investigation, formal analysis, Z.D. formal analysis, visualization. Y.L.: Formal analysis, methodology. Y.W.: Formal analysis, methodology. D.L.: Methodology X.Y.: Methodology, S.C.: Conceptualization, methodology, supervision, funding acquisition, writing—review and editing. H.P.: Conceptualization, methodology, resources, supervision, funding acquisition, writing—original draft, writing—review and editing. All authors reviewed the manuscript.

Acknowledgment

This work was supported by "Pioneer" and "Leading Goose" R&D Program of Zhejiang (2025C01099 and 2023C02040), National Key R&D Program of China (2022YFF1100204) and Jiashan Science and Technology Funds (2024A23).

References

1. Valdes, A. M.; Walter, J.; Segal, E.; Spector, T. D. Role of the Gut Microbiota in Nutrition and Health. *BMJ* 2018, *361*, k2179. https://doi.org/10.1136/bmj.k2179.
2. Kamada, N.; Chen, G. Y.; Inohara, N.; Nunez, G. Control of Pathogens and Pathobionts by the Gut Microbiota. *Nat. Immunol.* 2013, *14*, 685–690. https://doi.org/10.1038/ni.2608.
3. Raheel, I.; Orabi, A.; El-Hanbaly, S.; Shaheen, H. Action Mechanism and Immunity Status of Broiler Chickens after Spray and Drinking Water Administration of Kanne-Brottrunk®. *J. Appl. Environ. Microbiol.* 2018, *6*, 59–66. https://doi.org/10.12691/jaem-6-3-1.
4. Koirala, S.; Anal, A. K. Probiotics-Based Foods and Beverages as Future Foods and Their Overall Safety and Regulatory Claims. *Future Foods* 2021, *3*, 100013. https://doi.org/10.1016/j.fufo.2021.100013.
5. Dodoo, C. C.; Wang, J.; Basit, A. W.; Stapleton, P.; Gaisford, S. Targeted Delivery of Probiotics to Enhance Gastrointestinal Stability and Intestinal Colonisation. *Int. J. Pharm.* 2017, *530*, 224–229. https://doi.org/10.1016/j.ijpharm.2017.07.068.
6. Vargason, A. M.; Santhosh, S.; Anselmo, A. C. Surface Modifications for Improved Delivery and Function of Therapeutic Bacteria. *Small Weinh. Bergstr. Ger.* 2020, *16*, e2001705. https://doi.org/10.1002/smll.202001705.
7. Obradović, N.; Volić, M.; Nedović, V.; Rakin, M.; Bugarski, B. Microencapsulation of Probiotic Starter Culture in Protein–Carbohydrate Carriers Using Spray and Freeze-Drying Processes: Implementation in Whey-Based Beverages. *J. Food Eng.* 2022, *321*, 110948. https://doi.org/10.1016/j.jfoodeng.2022.110948.
8. Yang, C.; Cui, M.; Zhang, Y.; Pan, H.; Liu, J.; Wang, S.; Ma, N.; Chang, J.; Sun, T.; Wang, H. Upconversion Optogenetic Micro-Nanosystem Optically Controls the Secretion of Light-Responsive Bacteria for Systemic Immunity Regulation. *Commun. Biol.* 2020, *3*, 657. https://doi.org/10.1038/s42003-020-01415-0.
9. Hosseini, S. F.; Ansari, B.; Gharsallaoui, A. Polyelectrolytes-Stabilized Liposomes for Efficient Encapsulation of *Lactobacillus Rhamnosus* and Improvement of Its Survivability under Adverse Conditions. *Food Chem.* 2022, *372*, 131358. https://doi.org/10.1016/j.foodchem.2021.131358.
10. Gao, H.; Ma, L.; Sun, W.; McClements, D. J.; Cheng, C.; Zeng, H.; Zou, L.; Liu, W. Impact of Encapsulation of Probiotics in Oil-in-Water High Internal Phase Emulsions on Their Thermostability and Gastrointestinal Survival. *Food Hydrocoll.* 2022, *126*, 107478. https://doi.org/10.1016/j.foodhyd.2021.107478.

11. Sogut, E.; Filiz, B. E.; Seydim, A. C. Whey Protein Isolate- and Carrageenan-Based Edible Films as Carriers of Different Probiotic Bacteria. *J. Dairy Sci.* 2022, *105*, 4829–4842. https://doi.org/10.3168/jds.2021-21245.
12. Singh, P.; Medronho, B.; Miguel, M. G.; Esquena, J. On the Encapsulation and Viability of Probiotic Bacteria in Edible Carboxymethyl Cellulose-Gelatin Water-in-Water Emulsions. *FOOD Hydrocoll.* 2018, *75*, 41–50. https://doi.org/10.1016/j.foodhyd.2017.09.014.
13. Cook, M. T.; Tzortzis, G.; Charalampopoulos, D.; Khutoryanskiy, V. V. Microencapsulation of Probiotics for Gastrointestinal Delivery. *J. Control. Release Off. J. Control. Release Soc.* 2012, *162*, 56–67. https://doi.org/10.1016/j.jconrel.2012.06.003.
14. Wang, M.; Yang, J.; Li, M.; Wang, Y.; Wu, H.; Xiong, L.; Sun, Q. Enhanced Viability of Layer-by-Layer Encapsulated *Lactobacillus Pentosus* Using Chitosan and Sodium Phytate. *Food Chem.* 2019, *285*, 260–265. https://doi.org/10.1016/j.foodchem.2019.01.162.
15. Lee, H.; Kim, N.; Rheem, H. B.; Kim, B. J.; Park, J. H.; Choi, I. S. A Decade of Advances in Single-Cell Nanocoating for Mammalian Cells. *Adv. Healthc. Mater.* 2021, *10*, 2100347. https://doi.org/10.1002/adhm.202100347.
16. Anselmo, A. C.; McHugh, K. J.; Webster, J.; Langer, R.; Jaklenec, A. Layer-by-Layer Encapsulation of Probiotics for Delivery to the Microbiome. *Adv. Mater. Deerfield Beach Fla* 2016, *28*, 9486–9490. https://doi.org/10.1002/adma.201603270.
17. Cao, Z.; Cheng, S.; Wang, X.; Pang, Y.; Liu, J. Camouflaging Bacteria by Wrapping with Cell Membranes (Vol 10, 3452, 2019). *Nat. Commun.* 2022, *13*, 1520. https://doi.org/10.1038/s41467-022-28847-y.
18. Cao, Z.; Wang, X.; Pang, Y.; Cheng, S.; Liu, J. Biointerfacial Self-Assembly Generates Lipid Membrane Coated Bacteria for Enhanced Oral Delivery and Treatment. *Nat. Commun.* 2019, *10*, 5783. https://doi.org/10.1038/s41467-019-13727-9.
19. Priya, A. J.; Vijayalakshmi, S. P.; Raichur, A. M. Enhanced Survival of Probiotic Lactobacillus Acidophilus by Encapsulation with Nanostructured Polyelectrolyte Layers through Layer-by-Layer Approach. *J. Agric. Food Chem.* 2011, *59*, 11838–11845. https://doi.org/10.1021/jf203378s.
20. Cook, M. T.; Tzortzis, G.; Khutoryanskiy, V. V.; Charalampopoulos, D. Layer-by-Layer Coating of Alginate Matrices with Chitosan–Alginate for the Improved Survival and Targeted Delivery of Probiotic Bacteria after Oral Administration. *J. Mater. Chem. B* 2012, *1*, 52–60. https://doi.org/10.1039/C2TB00126H.
21. Rahim, M. A.; Kristufek, S. L.; Pan, S.; Richardson, J. J.; Caruso, F. Phenolic Building Blocks for the Assembly of Functional Materials. *Angew. Chem. Int. Ed Engl.* 2019, *58*, 1904–1927. https://doi.org/10.1002/anie.201807804.
22. Yi, Z.; Chen, G.; Chen, X.; Ma, X.; Cui, X.; Sun, Z.; Su, W.; Li, X. Preparation of Strong Antioxidative, Therapeutic Nanoparticles Based on Amino Acid-Induced Ultrafast Assembly of Tea Polyphenols. *ACS Appl. Mater. Interfaces* 2020, *12*, 33550–33563. https://doi.org/10.1021/acsami.0c10282.

23. Luo, H.; Wu, F.; Wang, X.; Lin, S.; Zhang, M.; Cao, Z.; Liu, J. Encoding Bacterial Colonization and Therapeutic Modality by Wrapping with an Adhesive Drug-Loadable Nanocoating. *Mater. Today* 2023, *62*, 98–110. https://doi.org/10.1016/j.mattod.2023.01.001.
24. Li, Y.; Miao, Y.; Yang, L.; Zhao, Y.; Wu, K.; Lu, Z.; Hu, Z.; Guo, J. Recent Advances in the Development and Antimicrobial Applications of Metal-Phenolic Networks. *Adv. Sci.* 2022, *9*, 2202684. https://doi.org/10.1002/advs.202202684.
25. Ejima, H.; Richardson, J. J.; Liang, K.; Best, J. P.; van Koeverden, M. P.; Such, G. K.; Cui, J.; Caruso, F. One-Step Assembly of Coordination Complexes for Versatile Film and Particle Engineering. *SCIENCE* 2013, *341*, 154–157. https://doi.org/10.1126/science.1237265.
26. Guo, H.; Zepeng, T.; Liying, X. U. E.; Qi, C.; Di, W.; Yanjiao, Y. I.; Meng, L. I.; Shujing, S. U. N.; Xiaonan, S. U. I. Effect of Interaction between EGCG and Soy β-Conglycinin/Glycinin on Protein Structure. *FOOD Sci.* 2022, *43*, 1. https://doi.org/10.7506/spkx1002-6630-20210508-081.
27. Poljanšek, I.; Krajnc, M. Characterization of Phenol-Formaldehyde Prepolymer Resins by In Line FT-IR Spectroscopy. *Acta Chim Slov* 2005.
28. Tan, S.; Han, J.; Yuan, X.; Song, Z.; Gao, L.; Gao, J.; Wang, L. Epigallocatechin Gallate-Loaded pH-Responsive Dressing with Effective Antioxidant, Antibacterial and Anti-Biofilm Properties for Wound Healing. *Mater. Des.* 2023, *227*, 111701. https://doi.org/10.1016/j.matdes.2023.111701.
29. Egerton, R. F.; Li, P.; Malac, M. Radiation Damage in the TEM and SEM. *Micron* 2004, *35*, 399–409. https://doi.org/10.1016/j.micron.2004.02.003.
30. Zhu, L.; Yu, T.; Wang, W.; Xu, T.; Geng, W.; Li, N.; Zan, X. Responsively Degradable Nanoarmor-Assisted Super Resistance and Stable Colonization of Probiotics for Enhanced Inflammation-Targeted Delivery. *Adv. Mater.* 2024, *36*. https://doi.org/10.1002/adma.202308728.
31. Yi, Z.; Chen, G.; Chen, X.; Sun, Z.; Ma, X.; Su, W.; Deng, Z.; Ma, L.; Ran, Y.; Tong, Q.; Li, X. Modular Assembly of Versatile Nanoparticles with Epigallocatechin Gallate. *ACS Sustain. Chem. Eng.* 2020, *8*, 9833–9845. https://doi.org/10.1021/acssuschemeng.0c02538.
32. Yu, L.; Lu, J.; Du, W. Tryptophan Metabolism in Digestive System Tumors: Unraveling the Pathways and Implications. *Cell Commun. Signal.* 2024, *22*, 174. https://doi.org/10.1186/s12964-024-01552-7.
33. Feng, T.; Wang, J. Oxidative Stress Tolerance and Antioxidant Capacity of Lactic Acid Bacteria as Probiotic: A Systematic Review. *Gut Microbes* 2020, *12*, 1801944. https://doi.org/10.1080/19490976.2020.1801944.
34. Chen, H.; Lei, P.; Ji, H.; Yang, Q.; Peng, B.; Ma, J.; Fang, Y.; Qu, L.; Li, H.; Wu, W.; Jin, L.; Sun, D. Advances in Escherichia Coli Nissle 1917 as a Customizable Drug Delivery System for Disease Treatment and Diagnosis Strategies. *Mater. Today Bio* 2023, *18*, 100543. https://doi.org/10.1016/j.mtbio.2023.100543.
35. Quideau, S.; Deffieux, D.; Douat-Casassus, C.; Pouységu, L. Plant Polyphenols: Chemical Properties, Biological Activities, and Synthesis. *Angew. Chem. Int. Ed Engl.* 2011, *50*, 586–621. https://doi.org/10.1002/anie.201000044.

36. Fan, G.; Wasuwanich, P.; Rodriguez-Otero, M. R.; Furst, A. L. Protection of Anaerobic Microbes from Processing Stressors Using Metal-Phenolic Networks. *J. Am. Chem. Soc.* 2022, *144*, 2438–2443. https://doi.org/10.1021/jacs.1c09018.
37. Yang, J.; Zhang, G.; Yang, X.; Peng, M.; Ge, S.; Tan, S.; Wen, Z.; Wang, Y.; Wu, S.; Liang, Y.; An, J.; Zhang, K.; Liu, J.; Shi, J.; Zhang, Z. An Oral "Super Probiotics" with Versatile Self-Assembly Adventitia for Enhanced Intestinal Colonization by Autonomous Regulating the Pathological Microenvironment. *Chem. Eng. J.* 2022, *446*, 137204. https://doi.org/10.1016/j.cej.2022.137204.
38. Fang, T.; Liu, S. Metal-Phenolic Network Directed Coating of Single Probiotic Cell Followed by Photoinitiated Thiol-Ene Click Fortification to Enhance Oral Therapy. *SMALL* 2024, *20*. https://doi.org/10.1002/smll.202308146.
39. Zhou, J.; Li, M.; Chen, Q.; Li, X.; Chen, L.; Dong, Z.; Zhu, W.; Yang, Y.; Liu, Z.; Chen, Q. Programmable Probiotics Modulate Inflammation and Gut Microbiota for Inflammatory Bowel Disease Treatment after Effective Oral Delivery. *Nat. Commun.* 2022, *13*, 3432. https://doi.org/10.1038/s41467-022-31171-0.
40. Feng, G.; Han, K.; Yang, Q.; Feng, W.; Guo, J.; Wang, J.; Yang, X. Interaction of Pyrogallol-Containing Polyphenols with Mucin Reinforces Intestinal Mucus Barrier Properties. *J. Agric. Food Chem.* 2022, *70*, 9536–9546. https://doi.org/10.1021/acs.jafc.2c03564.
41. Onoue, S.; Ochi, M.; Yamada, S. Development of (-)-Epigallocatechin-3-Gallate (EGCG)-Loaded Enteric Microparticles with Intestinal Mucoadhesive Property. *Int. J. Pharm.* 2011, *410*, 111–113. https://doi.org/10.1016/j.ijpharm.2011.03.020.
42. Luan, L.; Pan, H.; Chen, Y.; Ye, X.; Hou, Z.; Chen, S. Role of Extracted Phytochemicals from Rosa Sterilis S. D. Shi in DSS-Induced Colitis Mice: Potential Amelioration of UC. *Food Funct.* 2023, *14*, 8369–8382. https://doi.org/10.1039/D3FO02456C.
43. Yang, Y.; Ma, Q.; Wang, Q.; Zhao, L.; Liu, H.; Chen, Y. Mannose Enhances Intestinal Immune Barrier Function and Dextran Sulfate Sodium Salt-Induced Colitis in Mice by Regulating Intestinal Microbiota. *Front. Immunol.* 2024, *15*, 1365457. https://doi.org/10.3389/fimmu.2024.1365457.
44. Xie, W.-Y.; Ji, Z.-H.; Ren, W.-Z.; Zhao, P.-S.; Wei, F.-H.; Hu, J.; Yuan, B.; Gao, W. Wheat Peptide Alleviates DSS-Induced Colitis by Activating the Keap1–Nrf2 Signaling Pathway and Maintaining the Integrity of the Gut Barrier. *Food Funct.* 2024, *15*, 5466–5484. https://doi.org/10.1039/D3FO04413K.
45. Birchenough, G. M. H.; Nyström, E. E. L.; Johansson, M. E. V.; Hansson, G. C. INNATE IMMUNITY A sentinel goblet cell guards the colonic crypt by triggering Nlrp6-dependent Muc2 secretion. *Science* 2016, *352*, 1535–1542. https://doi.org/10.1126/science.aaf7419.
46. Eslam, M.; Newsome, P. N.; Sarin, S. K.; Anstee, Q. M.; Targher, G.; Romero-Gomez, M.; Zelber-Sagi, S.; Wai-Sun Wong, V.; Dufour, J.-F.; Schattenberg, J. M.; Kawaguchi, T.; Arrese, M. A New Definition for Metabolic Dysfunction-Associated Fatty Liver Disease: An International Expert Consensus Statement. *J. Hepatol.* 2020, *73*, 202–209. https://doi.org/10.1016/j.jhep.2020.03.039.
47. Guo, S.; Al-Sadi, R.; Said, H. M.; Ma, T. Y. Lipopolysaccharide Causes an Increase in Intestinal Tight Junction Permeability *in Vitro* and *in Vivo* by Inducing Enterocyte Membrane Expression and

Localization of TLR-4 and CD14. *Am. J. Pathol.* 2013, *182*, 375–387. https://doi.org/10.1016/j.ajpath.2012.10.014.

48. Sun, J.; Chen, H.; Kan, J.; Gou, Y.; Liu, J.; Zhang, X.; Wu, X.; Tang, S.; Sun, R.; Qian, C.; Zhang, N.; Niu, F.; Jin, C. Anti-Inflammatory Properties and Gut Microbiota Modulation of an Alkali-Soluble Polysaccharide from Purple Sweet Potato in DSS-Induced Colitis Mice. *Int. J. Biol. Macromol.* 2020, *153*, 708–722. https://doi.org/10.1016/j.ijbiomac.2020.03.053.
49. Günther, C.; Martini, E.; Wittkopf, N.; Amann, K.; Weigmann, B.; Neumann, H.; Waldner, M. J.; Hedrick, S. M.; Tenzer, S.; Neurath, M. F.; Becker, C. Caspase-8 Regulates TNF-α-Induced Epithelial Necroptosis and Terminal Ileitis. *Nature* 2011, *477*, 335–339. https://doi.org/10.1038/nature10400.
50. Neurath, M. F. Cytokines in Inflammatory Bowel Disease. *Nat. Rev. Immunol.* 2014, *14*, 329–342. https://doi.org/10.1038/nri3661.
51. Sanchez-Muñoz, F.; Dominguez-Lopez, A.; Yamamoto-Furusho, J. K. Role of Cytokines in Inflammatory Bowel Disease. *World J. Gastroenterol.* 2008, *14*, 4280. https://doi.org/10.3748/wjg.14.4280.
52. Ma, Y.; Jiang, S.; Zeng, M. *In Vitro* Simulated Digestion and Fermentation Characteristics of Polysaccharide from Oyster (Crassostrea Gigas), and Its Effects on the Gut Microbiota. *Food Res. Int.* 2021, *149*, 110646. https://doi.org/10.1016/j.foodres.2021.110646.
53. Jinbo, Y.; Taguchi, M.; Inoue, Y.; Kondo, H.; Miyasaka, T.; Tsujishita, H.; Sakamoto, F.; Tsukamoto, G. Synthesis and Antibacterial Activity of a New Series of Tetracyclic Pyridone Carboxylic Acids. *J. Med. Chem.* 1993, *36*, 3148–3153. https://doi.org/10.1021/jm00073a014.
54. Clavel, T.; Duck, W.; Charrier, C.; Wenning, M.; Elson, C.; Haller, D. Enterorhabdus Caecimuris Sp. Nov., a Member of the Family Coriobacteriaceae Isolated from a Mouse Model of Spontaneous Colitis, and Emended Description of the Genus Enterorhabdus Clavel et al. 2009. *Int. J. Syst. Evol. Microbiol.* 2010, *60*, 1527–1531. https://doi.org/10.1099/ijs.0.015016-0.

Scheme 1

Scheme 1 is available in the Supplementary Files section.

Figures

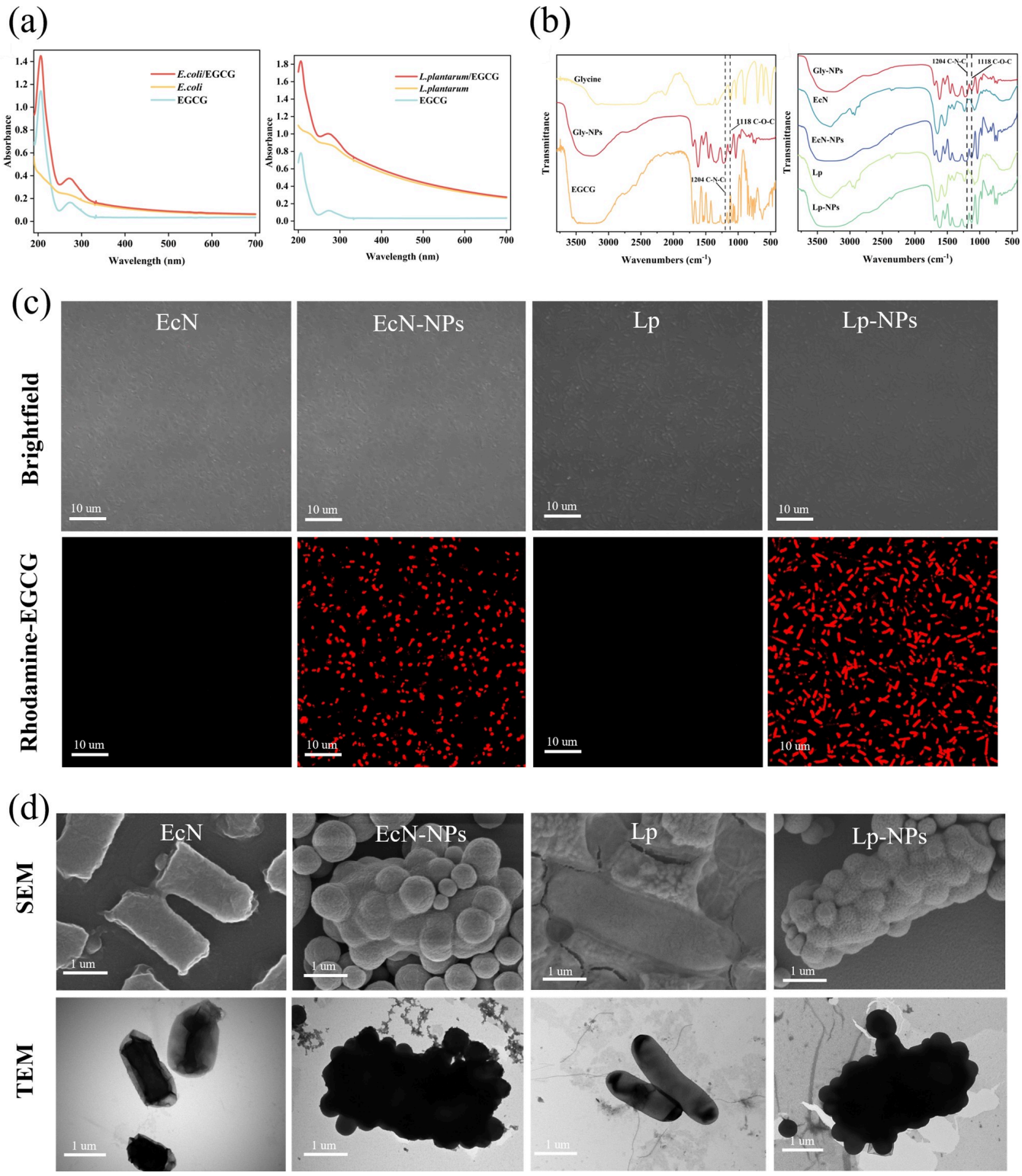


Figure 1

a) Ultraviolet-visible spectroscopy of EGCG adhered to the surface of probiotics. b) Fourier Transform Infrared Spectroscopy (FT-IR) spectra of nanoparticles formed by Mannich condensation reaction, as well as those of assembled bacteria and naked bacteria. c) Confocal Laser Scanning Microscopy (CLSM) images of assembled bacteria and naked bacteria, with rhodamine B-labeled EGCG shown in

red. Scale bar: 10 μm. d) Representative Scanning Electron Microscopy (SEM) and Transmission Electron Microscopy (TEM) images of EcN and Lp before and after assembly. Scale bar: 1 μm.

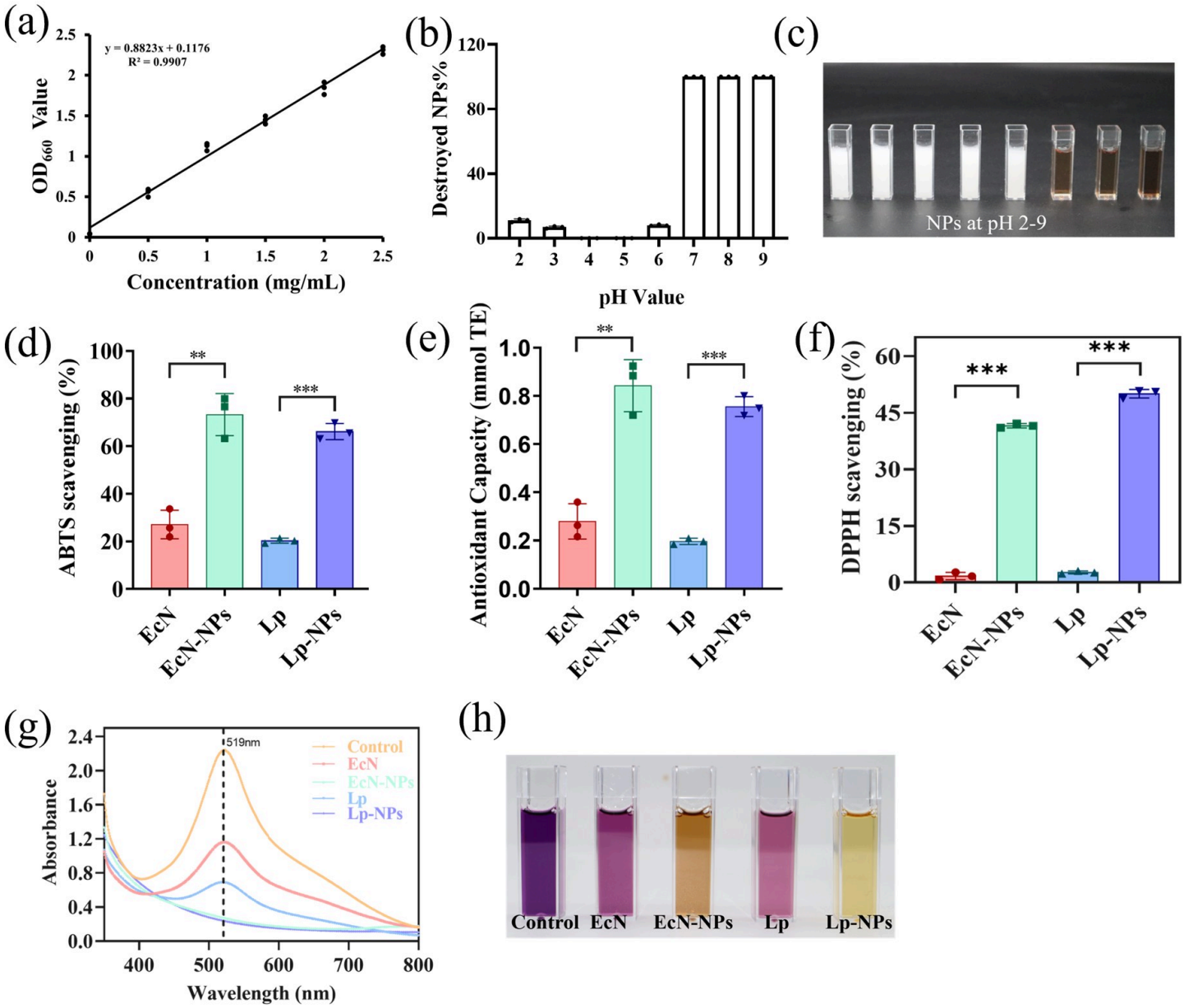


Figure 2

a) Linear relationship between the concentration of nanoparticles and the OD value at 660 nm. b) Disassembly rate of nanoparticles at different pH values and c) corresponding images. d) ABTS scavenging rate, e) antioxidant capacity, f, g, h) DPPH scavenging effect of assembled bacteria and naked bacteria. *p< 0.05, **p < 0.01, ***p < 0.001.

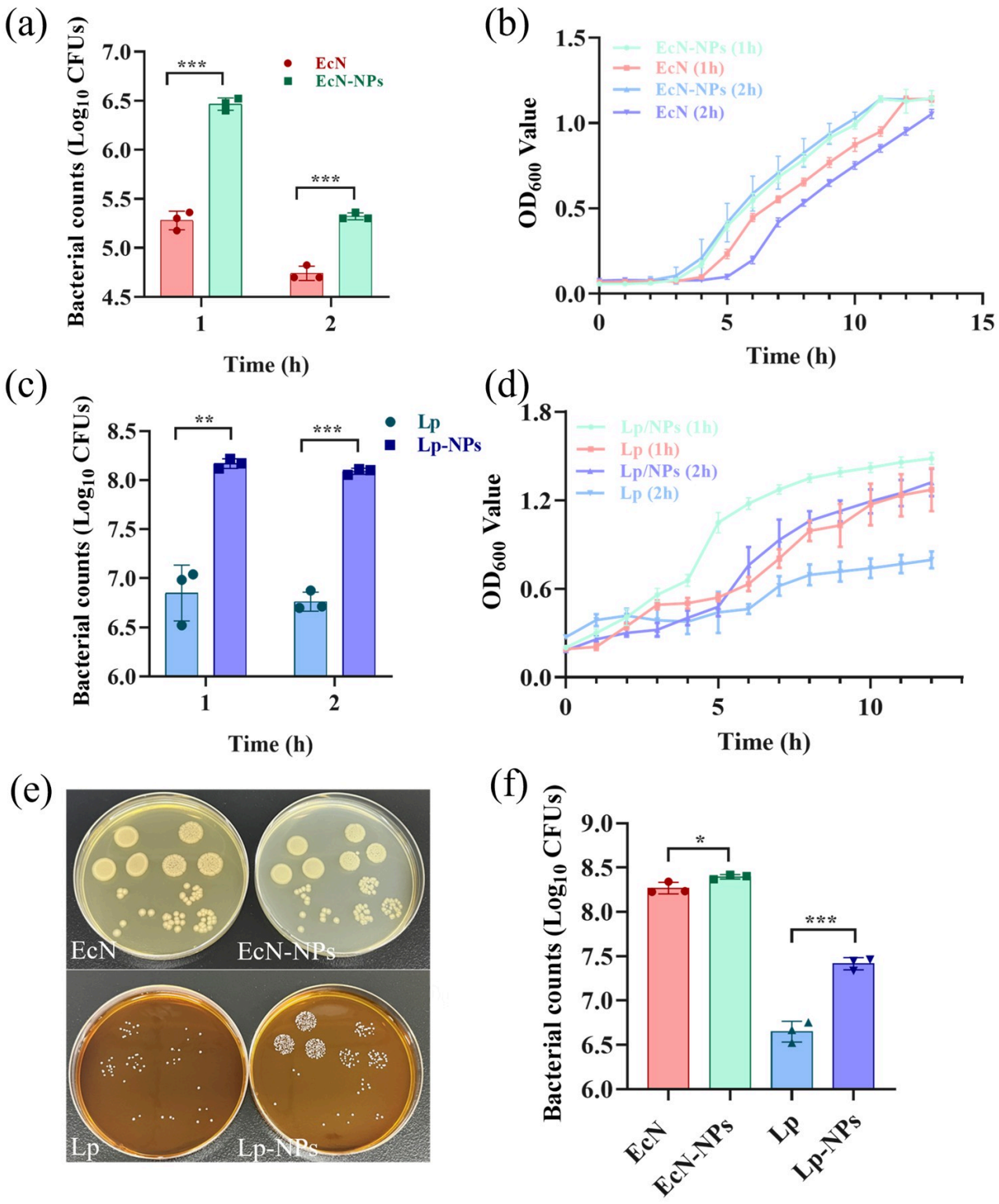


Figure 3

Resistance in simulated gastrointestinal fluids in vitro. Viability of naked bacteria and assembled bacteria after treatment with simulated gastric fluid: a, b) EcN; c, d) Lp. e, f) Plate count of assembled bacteria and naked bacteria after 2-hour treatment with simulated intestinal fluid. *$p < 0.05$, **$p < 0.01$, ***$p < 0.001$.

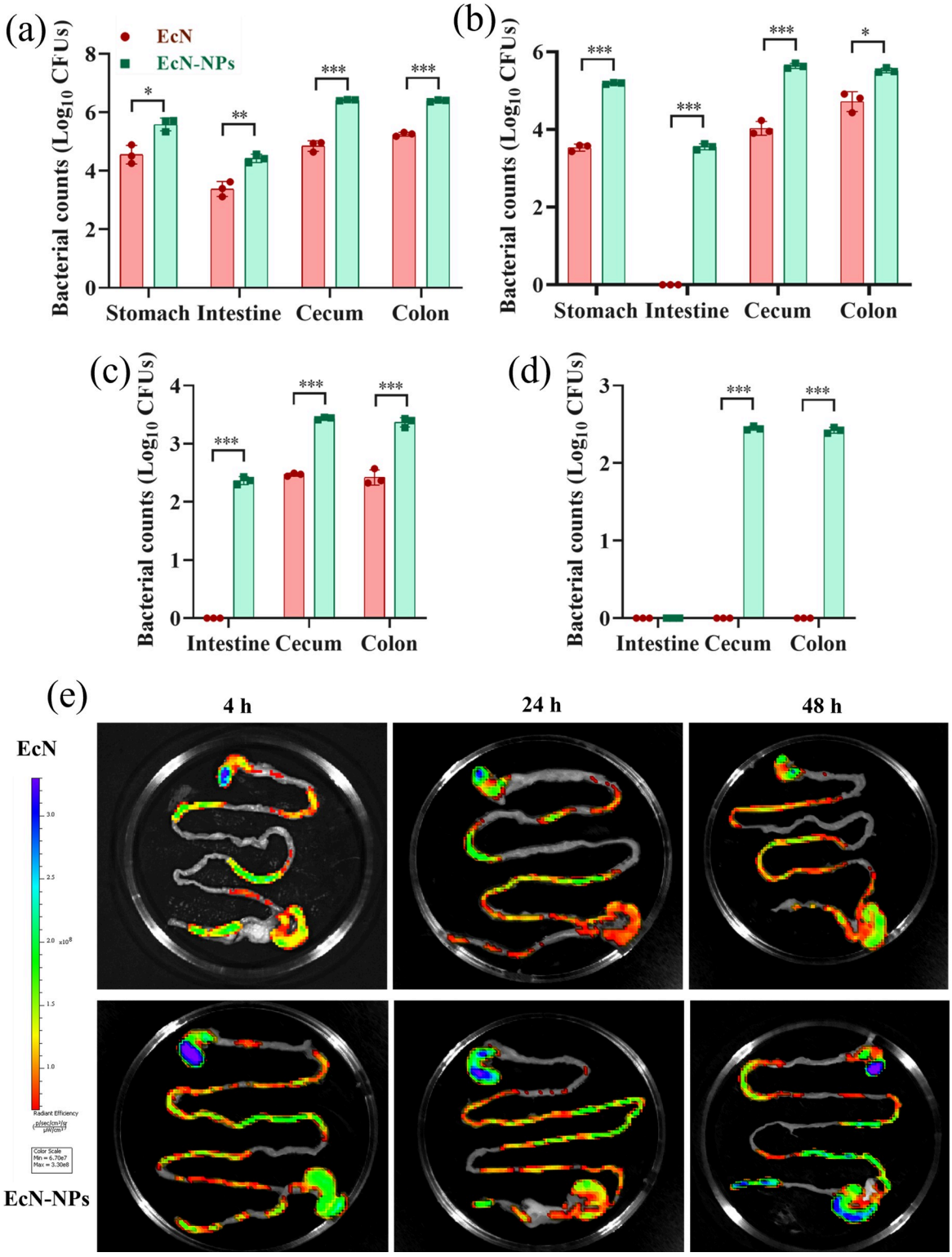


Figure 4

Colonization and survival of probiotics in the mouse gastrointestinal tract. The survival rates of naked and assembled EcN in the mouse gastrointestinal tissues (stomach, small intestine, colon, and cecum) at a) 4 h, b) 24 h, c) 48 h, and d) 96 h after oral administration. e) IVIS bioluminescence images of the mouse gastrointestinal tract at 4 h, 24 h, and 48 h after oral administration of naked or armed EcN carrying pBBR1MCS2-Tac-mCherry. *$p < 0.05$, **$p < 0.01$, ***$p < 0.001$.

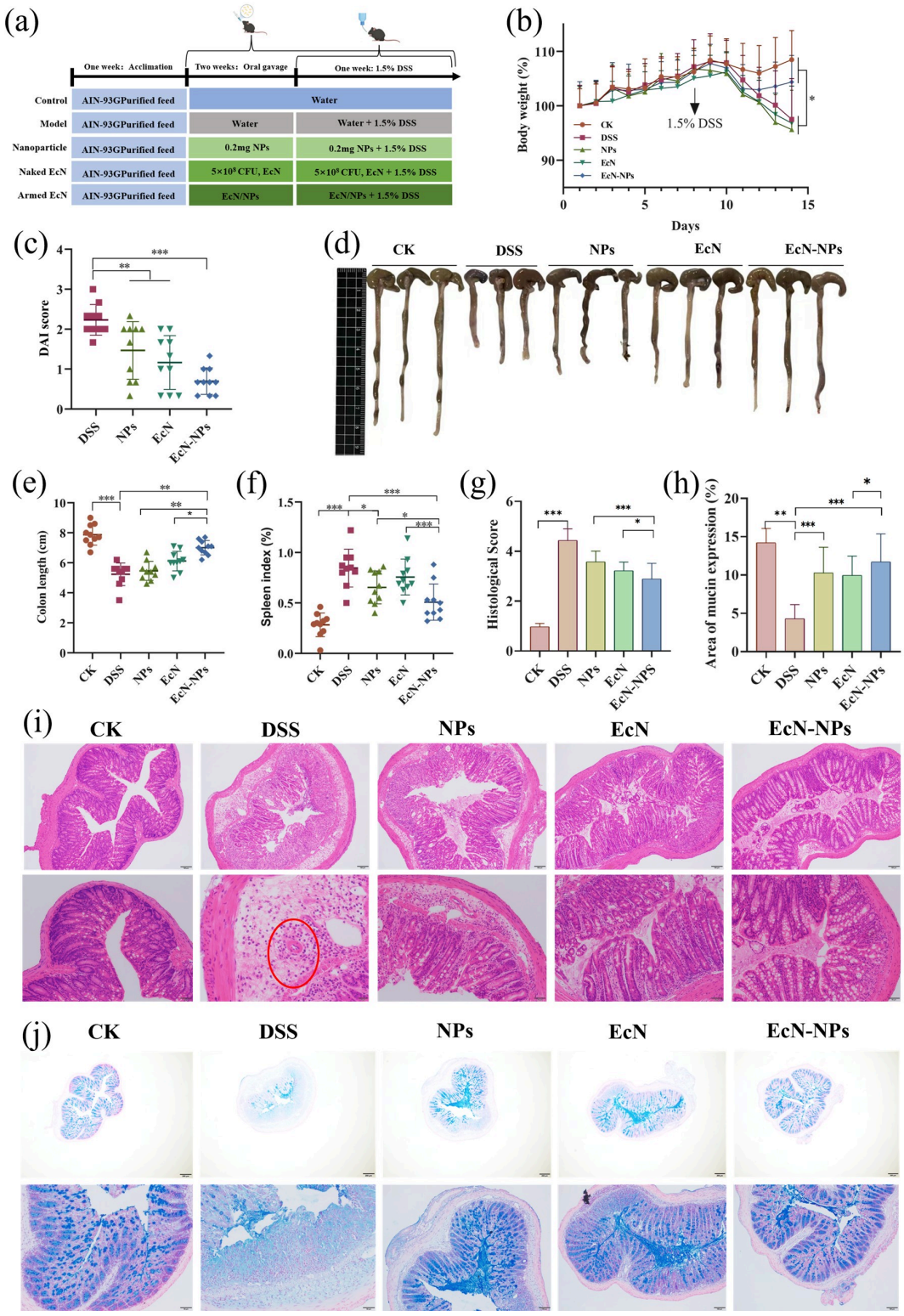


Figure 5

Oral administration of assembled EcN alleviates DSS-induced colitis in mice. a) Schematic diagram of the mouse modeling and treatment process. b) Changes in body weight of mice during the 14-day experiment. c) The DAI of the mice. d, e) Photos of the mouse colon length and colon tissue, respectively. f) The spleen index of the mice. g, h) Representative images and tissue scores of colon tissues stained with hematoxylin-eosin (H&E). Scale bar: 100 μm. i, g) Representative images and

proportion of mucin area of colon tissues stained with Alcian Blue (AB) staining. *$p < 0.05$, **$p < 0.01$, ***$p < 0.001$.

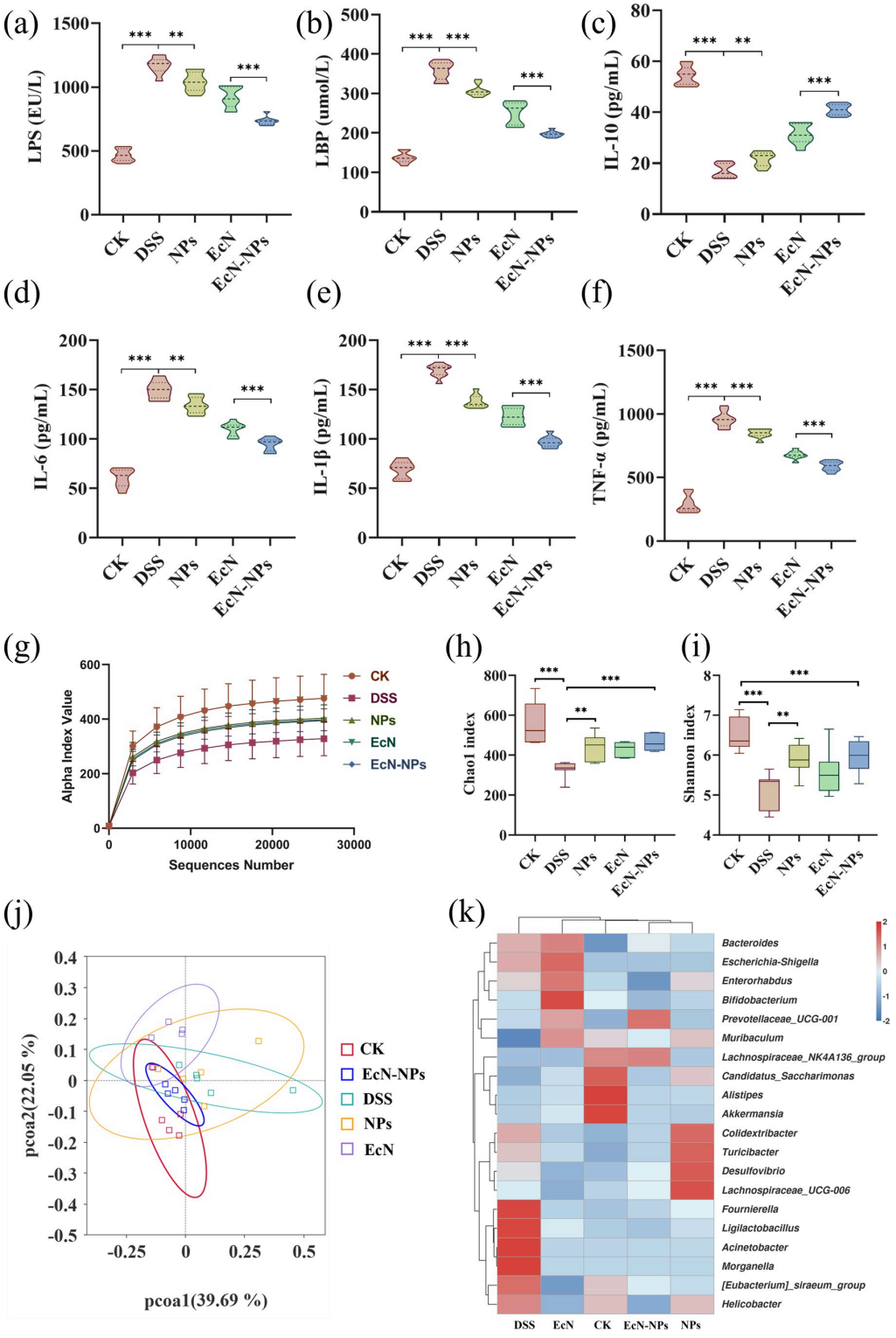


Figure 6

Expression of inflammatory factors in the serum of mouse eyeballs: a) Lipopolysaccharide (LPS); b) Lipopolysaccharide-binding protein (LBP); c) Anti-inflammatory factor IL-10; d-f) Pro-inflammatory factors TNF-α, IL-6, and IL-1β. 16S rRNA sequencing of the intestinal microbiota in mice of different

treatment groups: g) Rarefaction curves; Diversity indices: h) Chao 1 and i) Shannon; j) Principal Coordinates Analysis (PCoA) plot demonstrating the diversity of the gut microbiota; k) Heatmap of the relative abundances of the top 20 gut microbiota classified at the genus level.*$p < 0.05$, **$p < 0.01$, ***$p < 0.001$.

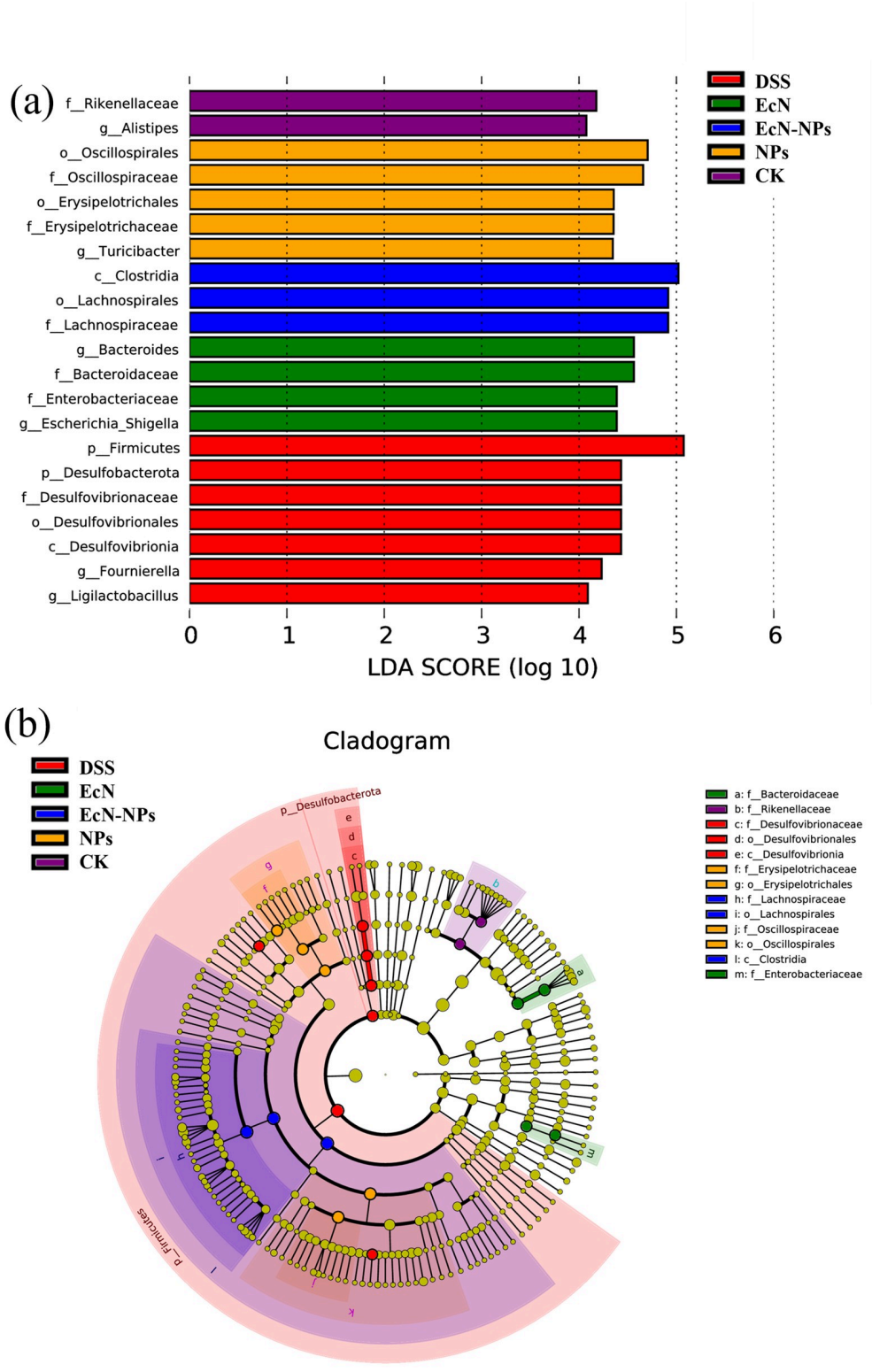


Figure 7

The LDA score plot a) and the cladogram b) of LEfSe analysis of the mouse gut microbiota, with LDA > 4.

Supplementary Files

This is a list of supplementary files associated with this preprint. Click to download.

- Supportinginformation.docx
- scheme1.jpg